Available online at www.sciencedirect.com

SciVerse ScienceDirect

Ceramics International 38 (2012) 1489–1495

CERAMICS INTERNATIONAL

www.elsevier.com/locate/ceramint

Tunable luminescence properties and efficient energy transfer in Eu^{2+},Mn^{2+} co-doped $Ba_2MgP_4O_{13}$

Nuan Xie [a], Jinyin Liu [a], Yanlin Huang [a], Sun Il Kim [b,*], Hyo Jin Seo [b,*]

[a] College of Chemistry, Chemical Engineering and Materials Science, Soochow University, Suzhou 215123, China
[b] Department of Physics, Pukyong National University, Busan 608-737, Republic of Korea

Received 1 August 2011; received in revised form 2 September 2011; accepted 2 September 2011
Available online 17 September 2011

Abstract

A series of $Ba_2Mg_{1-x}Mn_xP_4O_{13}$ ($x = 0$–1.0) and $Ba_{1.94}Eu_{0.06}Mg_{1-x}Mn_xP_4O_{13}$ ($x = 0$–0.15) phosphors were prepared by conventional solid-state reaction. X-ray powder diffraction (XRD), the photoluminescence spectra, and the decay curves are investigated. XRD analysis shows that the maximum tolerable substitution of Mn^{2+} for Mg is about 50 mol% in $Ba_2MgP_4O_{13}$. Mn^{2+}-singly doped $Ba_2MgP_4O_{13}$ shows weak red-luminescence peaked at about 615 nm. The Eu^{2+}/Mn^{2+} co-doped phosphor emits two distinctive luminescence bands: a blue one centered at 430 nm originating from Eu^{2+} and a broad red-emitting one peaked at 615 nm from Mn^{2+} ions. The luminescence of Mn^{2+} ions can be greatly enhanced with the co-doping of Eu^{2+} in $Ba_2MgP_4O_{13}$. The efficient energy transfer from Eu^{2+} to Mn^{2+} is verified by the excitation and emission spectra together with the luminescence decay curves. The emission colors could be tuned from the blue to the red-purple and eventually to the deep red. The resonance-type energy transfer via a dipole–quadrupole interaction mechanism is supported by the decay lifetime data. The energy transfer efficiency and the critical distance are calculated and discussed. The temperature dependent luminescence spectra of the Eu^{2+}/Mn^{2+} co-doped phosphor show a good thermal stability on quenching effect.

Keywords: Phosphate; Mn^{2+}; Luminescence; White light-emitting diodes

1. Introduction

Mn^{2+} ions have been widely investigated in the materials for the luminescent [1–4], electrical [5], magnetic [6], and mechanical [7] properties, etc. The typical luminescence of Mn^{2+} ($3d^5$) is attributed to the $^4T_1 \rightarrow {}^6A_1$ transitions. From the Tanabe–Sugano diagram, the emission transition of $^4T_{1g}(G) \rightarrow {}^6A_{1g}(G)$ in Mn^{2+} ions depends on the crystal field strength of the substituted sites [8]. For example, the Mn^{2+} in tetrahedral coordination usually gives a green emission, whereas Mn^{2+} with octahedral coordination gives a red emission. This gives a wide usage of Mn^{2+}-doped compounds for fluorescent lamps, cathode ray tubes and white light-emitting diodes (LEDs) [9,10].

As described in the Sugano–Tanabe diagram the ground state of Mn^{2+} has six manifold spin degeneracy. However, no excited states of Mn^{2+} have sextet spin degeneracy [8]. As a result, all the absorption transitions to the excited state are spin-forbidden with low transition probabilities. In order to increase the emission intensity, a sensitizer has to be used to increase the excitation of Mn^{2+} ions, e.g., Eu^{2+} [11,12] or Ce^{3+} [13]; since the energy levels of excited states from Mn^{2+} match with some energy levels of Eu^{2+} and Ce^{3+} ions, the energy transfer from Eu^{2+} or Ce^{3+} to Mn^{2+} has been studied extensively in many hosts, for example, silicates [14–16], borates [17], aluminates [18], and phosphates [19]. Among these phosphors, Eu^{2+}/Mn^{2+} co-doped phosphates have been paid great attention because the efficient energy transfer could occur from Eu^{2+} to Mn^{2+}, for example, $Ca_9Gd(PO_4)_7$:Eu^{2+},Mn^{2+} [20,21], $Ca_9Y(PO_4)_7$:Eu^{2+},Mn^{2+} [22], $Ca_9Lu(PO_4)_7$:Eu^{2+},Mn^{2+} [23], $Ca_9Y(PO_4)_7$:Ce^{3+},Mn^{2+} [24], $Ca_8MgLa(PO_4)_7$:Ce^{3+},Mn^{2+} [25], $(Ca,Mg,Sr)_9Y(PO_4)_7$:Eu^{2+},Mn^{2+} [26], $Ca_6Mg(PO_4)_4$:Eu^{2+},Mn^{2+} [27], $Ca_{10}K(PO_4)_7$:Eu^{2+},Mn^{2+} [28], $Ca_2P_2O_7$:Eu^{2+},Mn^{2+} [29,30], and $(Sr,Ca)_2P_2O_7$:Eu^{2+},Mn^{2+} [31], etc. These phosphates are considered to be the excellent phosphors for W-LEDs. Eu^{2+} ions can absorb UV or near-UV light (n-UV), and Mn^{2+} can give an enhanced red emission through $Eu^{2+} \rightarrow Mn^{2+}$ energy transfer.

Recently Eu^{2+}-activated $Ba_2MgP_4O_{13}$ has been reported to have the efficient blue luminescence and an excellent thermal

* Corresponding authors.
E-mail addresses: sikim@pknu.ac.kr (S.I. Kim), hjseo@pknu.ac.kr (H.J. Seo).

0272-8842/$36.00
doi:10.1016/j.ceramint.2011.09.032

stability against the temperature quenching. It is a potential blue-emitting phosphor for the application in n-UV based W-LEDs [32]. In this work, the phase formation, and luminescence colors of Mn^{2+}-doped and Eu^{2+}/Mn^{2+} co-doped $Ba_2MgP_4O_{13}$ are studied. Mn^{2+}-singly doped $Ba_2MgP_4O_{13}$ presents weak red luminescence, which can be greatly enhanced by Eu^{2+} co-doping due to the efficient energy transfer from Eu^{2+} to Mn^{2+}. $Ba_2MgP_4O_{13}$:Eu^{2+},Mn^{2+} phosphors with the variation of Mn^{2+} were synthesized and examined by XRD and photoluminescence spectra. The luminescence properties, color chromaticity and energy transfer phenomenon are discussed.

2. Experimental

Polycrystalline samples of $Ba_2Mg_{1-x}Mn_xP_4O_{13}$ ($x = 0$, 0.01, 0.03, 0.05, 0.07, 0.1, 0.12, 0.15, 0.30, 0.50, 0.60, 0.85, 1.0) and $Ba_{1.94}Eu_{0.06}Mg_{1-x}Mn_xP_4O_{13}$ ($x = 0$, 0.01, 0.03, 0.05, 0.07, 0.1, 0.12, 0.15) were prepared by high temperature solid-state reaction method. The starting material was a stoichiometric mixture of reagent grade $C_4Mg_4O_{12}$–$H_2MgO_2{\cdot}5H_2O$ (magnesium carbonate basic pentahydrate), $BaCO_3$, $NH_4H_2PO_4$, $MnCO_3$ and Eu_2O_3.

Firstly, the mixture was heated up to 350 °C and kept at this temperature for 6 h. The powder obtained was thoroughly mixed in acetone and then heated up to 850 °C and kept at this temperature for 5 h in air. After that, the sample was thoroughly mixed and heated in air at 1050 °C for 10 h in a reducing atmosphere.

XRD were collected on a Rigaku D/Max diffractometer operating at 40 kV, 30 mA with Bragg-Brentano geometry using Cu Kα radiation (λ = 1.5405 Å). The excitation and luminescence spectra were recorded on a Perkin-Elmer LS-50B luminescence spectrometer with Monk-Gillieson type monochromators and a xenon discharge lamp used as the excitation source. The luminescence decay curves were measured by the excitation of 355 nm pulsed Nd:YAG laser (Spectron Laser Sys. SL802G). The signals were recorded by the 500 MHz digital oscilloscope (Tektronix DPO 3054).

3. Results and discussion

3.1. The phase formation

Considering the ionic radius of Ba^{2+} (1.42 Å), Mg^{2+} (0.72 Å), Eu^{2+} (1.25 Å) and Mn^{2+} (0.83 Å), it is predicted that Eu^{2+} and Mn^{2+} prefer to occupy the Ba^{2+} and Mg^{2+} sites in $Ba_2MgP_4O_{13}$, respectively. Fig. 1 shows the XRD patterns of $Ba_2Mg_{1-x}Mn_xP_4O_{13}$ ($x = 0$, 0.01, 0.03, 0.05, 0.07, 0.1, 0.12, 0.15, 0.30, 0.50, 0.60, 0.85, 1.0) and JCPDs Card No. 16-0640 ($Ba_2MgP_4O_{13}$). The XRD patterns of the samples with $x = 0$–0.5 are consistent with JCPDs Card No. 16-0640 ($Ba_2MgP_4O_{13}$) and can be indexed to single phase orthorhombic $Ba_2MgP_4O_{13}$ [33]. This indicates that the doping of Mn^{2+} ($x \leq 0.5$) does not significantly change the phase structure of samples.

However, several extra refraction peaks were observed on the XRD pattern of sample $Ba_2Mg_{1-x}Mn_xP_4O_{13}$ ($x > 0.5$). The relative intensities of these extra peaks steadily increase with

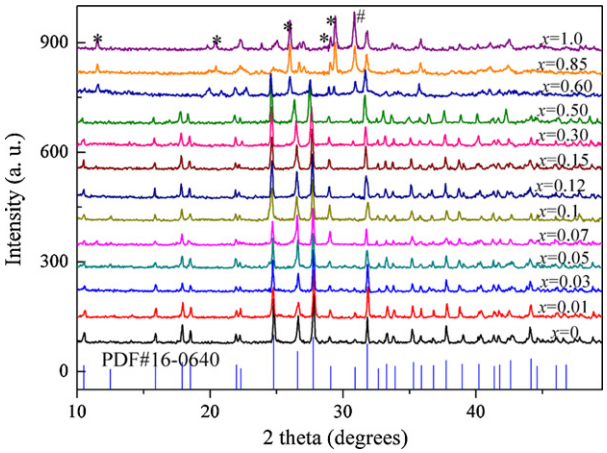

Fig. 1. XRD patterns of $Ba_2Mg_{1-x}Mn_xP_4O_{13}$ ($x = 0$, 0.01, 0.03, 0.05, 0.07, 0.1, 0.12, 0.15, 0.30, 0.50, 0.60, 0.85, 1.0) and JCPDs Card No. 16-0640 ($Ba_2MgP_4O_{13}$). * and # denote the appearance of impurity phases of $BaMn(PO_3)_4$ and $Ba_3(PO_4)_2$, respectively.

increasing x-value above 0.5. By searching and comparing the extra refraction patterns with the data base of standard JCPDs Cards for inorganic materials, the main impurities formed in samples are the new crystal phases of $BaMn(PO_3)_4$ (PDF#29-0189) and $Ba_3(PO_4)_2$ (PDF#24-0116). The syntheses of these samples were repeated for three times. The results indicate that the impurity phases always appear when the doping of Mn^{2+} exceeds 50 mol%. The experimental results confirm that the maximum tolerable substitution of Mn^{2+} for Mg^{2+} is 50 mol%.

3.2. The concentration dependent emission spectra and decay

The concentration dependence of the emission spectra on the Mn^{2+} doping is investigated. The emission spectra of $Ba_2Mg_{1-x}Mn_xP_4O_{13}$ ($x = 0.01$–0.85) are shown in Fig. 2. All the spectra of $Ba_2Mg_{1-x}Mn_xP_4O_{13}$ ($x = 0.01$, 0.03, 0.05, 0.07, 0.1, 0.12, 0.15, 0.30, 0.50) show a broad emission centered at about 615 nm, due to the $^4T_1$–$^6A_1$ transitions of Mn^{2+} ions (the luminescence spectra of $Ba_2Mg_{1-x}Mn_xP_4O_{13}$ ($x = 0.30$, 0.50) were not shown in Fig. 2 for a conciseness). The luminescence

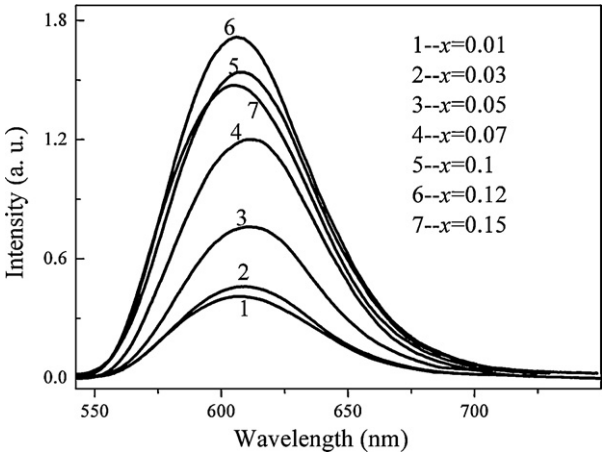

Fig. 2. The luminescence spectra of $Ba_2Mg_{1-x}Mn_xP_4O_{13}$ ($x = 0.01$, 0.03, 0.05, 0.07, 0.1, 0.12, 0.15).

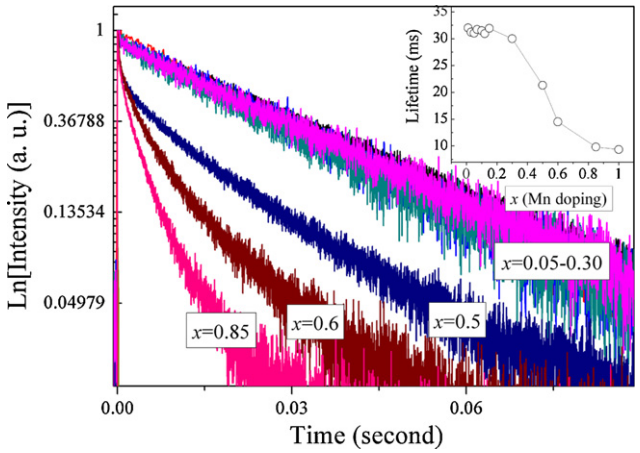

Fig. 3. The luminescence decay curves of $Ba_2Mg_{1-x}Mn_xP_4O_{13}$ ($x = 0.05$–0.85); the inset shows the dependence of lifetime values on the Mn^{2+} doping.

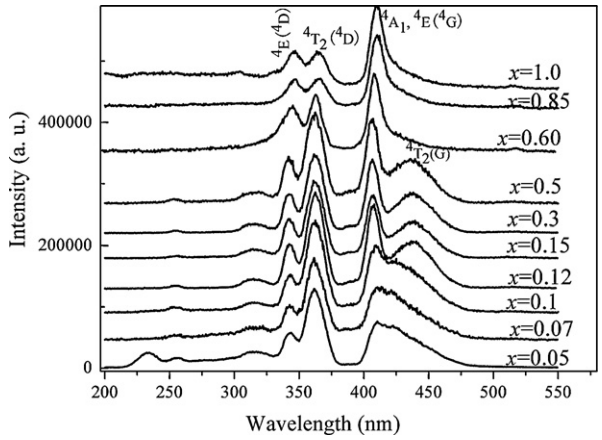

Fig. 4. The excitation spectra of $Ba_2Mg_{1-x}Mn_xP_4O_{13}$ ($x = 0.05$–1.0). The transitions from the ground state $^6A_{1g}(S)$ to the excited states are labeled.

is enhanced with increasing Mn^{2+}-concentration until the maximum intensity reaches at $x = 0.12$, and then it decreases at the concentration higher than 12 mol% because of the concentration quenching.

Fig. 3 shows the luminescence decay curves of Mn^{2+} ions in $Ba_2Mg_{1-x}Mn_xP_4O_{13}$ ($x = 0.05$–0.85). The luminescence curves of $Ba_2Mg_{1-x}Mn_xP_4O_{13}$ ($x = 0.05$–0.3) present good single exponential decay profiles, which are well fitted by a single exponential equation:

$$I = A_1 \exp\left(-\frac{t}{\tau}\right) \quad (1)$$

However, the other curves could not be fitted by a single exponential process, which show fast decay at the initial stage and then slow decay at the later time region. The non-exponential decay curves of $Ba_2Mg_{1-x}Mn_xP_4O_{13}$ ($x = 0.5$–0.85) can be fitted to the effective lifetime defined as the following [34]:

$$\tau_{average} = \frac{\int_0^\infty I(t)tdt}{\int_0^\infty I(t)dt} \quad (2)$$

where $I(t)$ represents the luminescence intensity at a time t after the cutoff of the excitation light. The lifetime values are displayed in inset in Fig. 3.

The emission of $Ba_2Mg_{1-x}Mn_xP_4O_{13}$ ($x = 0.05$–0.3) keeps the nearly constant lifetime values, which are typical for the parity and spin forbidden $^4T_1 \rightarrow {}^6A_1$ transition of Mn^{2+} [35]. However, it decreases fast with increasing Mn^{2+} doping. The fast component is attributed to the rapid energy transfer from Mn^{2+} ion to closely spaced neighbor Mn^{2+} ion, which are shorter and shorter as the Mn^{2+} concentration increases. It has been reported that an increase of Mn^{2+} concentration produces a decrease of Mn^{2+} luminescence lifetime [36]. This was explained in terms of cross-relaxation interactions between the close Mn^{2+} pairs.

3.3. The excitation spectra of Eu^{2+} and Mn^{2+}

The excitation and emission spectra of Eu^{2+}-doped $Ba_2MgP_4O_{13}$ have been recently reported [32]. The excitation band of Eu^{2+} locates in a wavelength range 250–400 nm, indicating that this phosphor can be well excited at the wavelength range from deep UV to near UV. The $Ba_2MgP_4O_{13}$:Eu^{2+} phosphor shows an intense blue emission band peaking at 430 nm.

The excitation spectra of $Ba_2Mg_{1-x}Mn_xP_4O_{13}$ ($x = 0.05$–1.0) are shown in Fig. 4. The bands are attributed to the *d–d* transitions of Mn^{2+}; it consists of several absorption bands associated with Mn^{2+} transition from the ground state $^6A_{1g}(S)$ to the excited states $^4T_{1g}(G)$, $^4T_{2g}(G)$, $[^4A_{1g}(G)$, $^4E_g(G)]$, $^4T_{2g}(D)$, $^4E_g(D)$, $^4T_{1g}(P)$, $^4A_{2g}(F)$, $^4T_{1g}(F)$, and $^4T_{2g}(F)$. Even the corresponding transitions are spin-forbidden, the absorption bands from 350 to 450 nm for the Mn^{2+}-doped $Ba_2Mg_{1-x}Mn_xP_4O_{13}$ ($x = 0.05$–1.0) can be detected.

Under the UV lamp excitation, the Mn^{2+}-singly doped samples show weak pink-red color. However, the Eu^{2+}/Mn^{2+} co-doped samples display bright luminescence. Fig. 5(a) and (b) shows the luminescence spectra of Mn^{2+}-singly doped $Ba_2Mg_{1-x}Mn_xP_4O_{13}$ ($x = 0.10$) and Eu^{2+}/Mn^{2+} co-doped $Ba_{1.94}Eu_{0.06}Mg_{1-x}Mn_xP_4O_{13}$ ($x = 0.1$), respectively. Under

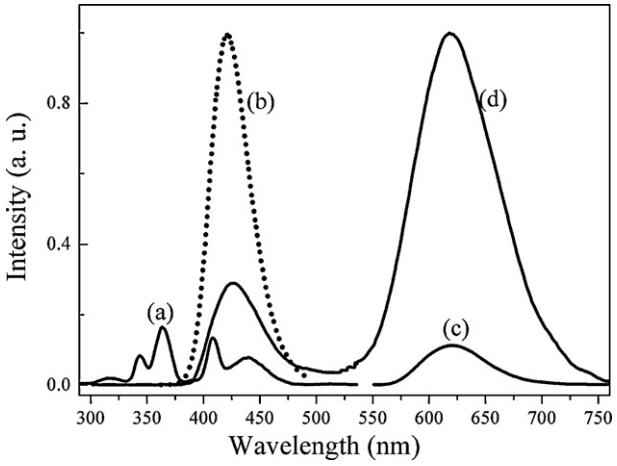

Fig. 5. The luminescence spectra of Mn^{2+}-singly doped $Ba_2Mg_{1-x}Mn_xP_4O_{13}$ ($x = 0.1$) (a) and Eu^{2+}/Mn^{2+} co-doped $Ba_{1.94}Eu_{0.06}Mg_{1-x}Mn_xP_4O_{13}$ ($x = 0.1$) (b); the excitation spectra of $Ba_2Mg_{1-x}Mn_xP_4O_{13}$ ($x = 0.1$) (c); and the luminescence spectrum of $Ba_{1.94}Eu_{0.06}MgP_4O_{13}$ (d).

the same measurement conditions, the luminescence intensity of Mn^{2+} in $Ba_{1.94}Eu_{0.06}Mg_{1-x}Mn_xP_4O_{13}$ ($x = 0.1$) is greatly enhanced in comparison with that of $Ba_2Mg_{1-x}Mn_xP_4O_{13}$ ($x = 0.1$). This indicates that the efficient energy transfer takes place from Eu^{2+} to Mn^{2+} ions, which can be also approved by the good spectra overlap between the excitation of $Ba_2Mg_{1-x}Mn_xP_4O_{13}$ ($x = 0.1$) (Fig. 5(c)) and the luminescence spectrum of $Ba_{1.94}Eu_{0.06}MgP_4O_{13}$ (Fig. 5(d)) in the region of 400–450 nm. On the other hand, the emission spectrum of $Ba_{1.94}Eu_{0.06}Mg_{1-x}Mn_xP_4O_{13}$ ($x = 0.1$) (Fig. 5(d)) consists of two broad emission bands centered at 430 and 615 nm, originating from the Eu^{2+} and Mn^{2+}, respectively.

3.4. The energy transfer from Eu^{2+} to Mn^{2+}

The luminescence spectra for Eu^{2+}/Mn^{2+} co-doped phosphors $Ba_{1.94}Eu_{0.06}Mg_{1-x}Mn_xP_4O_{13}$ ($x = 0$–0.15) are shown in Fig. 6(a). The integrated luminescence intensities of Eu^{2+} and Mn^{2+} ions were calculated and shown in Fig. 6(b). With increasing Mn^{2+} concentration up to 10 mol%, the emission intensity of the Eu^{2+} decreases drastically, whereas the red-emission of Mn^{2+} increases. This could be the evidence that the effective energy transfer from Eu^{2+} to Mn^{2+} takes place.

Furthermore, the decay curves of $Ba_{1.94}Eu_{0.06}Mg_{1-x}Mn_xP_4O_{13}$ monitored at 430 nm (Eu^{2+} emission) are shown in Fig. 7(a). The decay curve of $Ba_{1.94}Eu_{0.06}MgP_4O_{13}$ is single exponential, which can be well fit in Eq. (1). However, the decay curves of Eu^{2+} emission in the Eu^{2+}/Mn^{2+} co-doped samples could not be fitted by a single exponential process, which can be fitted to the effective lifetime as defined in Eq. (2). The decay lifetime τ of Eu^{2+} emission reduced monotonically from 0.54 to 0.086 μs as x increased from 0 to 0.15. The energy transfer efficiency η_T from Eu^{2+} to Mn^{2+} has been reported to be expressed by the following formula [37]:

$$\eta_T = 1 - \frac{\tau_S}{\tau_{S0}} \cong 1 - \frac{I_S}{I_{S0}} \tag{3}$$

where τ_{S0} and τ_S are the decay lifetimes of the sensitizer (Eu^{2+}) in the absence and presence of the activator (Mn^{2+}), respectively. I_{S0} and I_S are the luminescence intensities of the sensitizer Eu^{2+} in the absence and presence of the activator Mn^{2+}, respectively. η_T, the energy transfer efficiency from Eu^{2+} to Mn^{2+} in $Ba_{1.94}Eu_{0.06}Mg_{1-x}Mn_xP_4O_{13}$, calculated as a function of x, is shown in Fig. 7(b). With increasing Mn^{2+} dopant content, the η_T is found to increase and reach the saturation when x is above 0.15.

On the base of the Dexter's energy transfer formula of multipolar interaction and Reisfeld's approximation, the following relation can be obtained [38,39]:

$$\frac{\eta_{S0}}{\eta_S} \propto C^{\alpha/3} \quad \text{and} \quad \frac{I_{S0}}{I_S} \propto C^{\alpha/3} \tag{4}$$

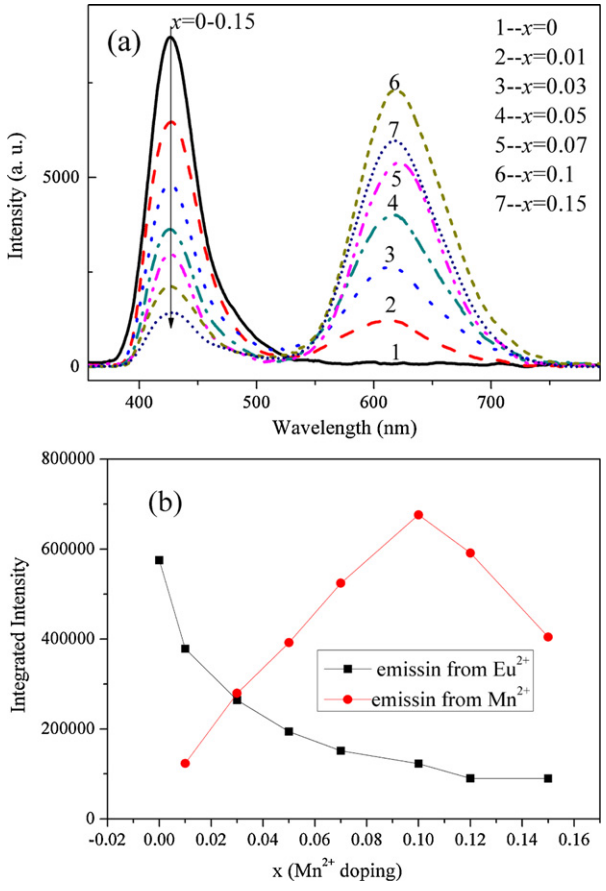

Fig. 6. (a) The emission spectra of $Ba_{1.94}Eu_{0.06}Mg_{1-x}Mn_xP_4O_{13}$ ($x = 0$–0.15) excited at 355 nm; (b) the integrated emission intensities of Eu^{2+} and Mn^{2+}.

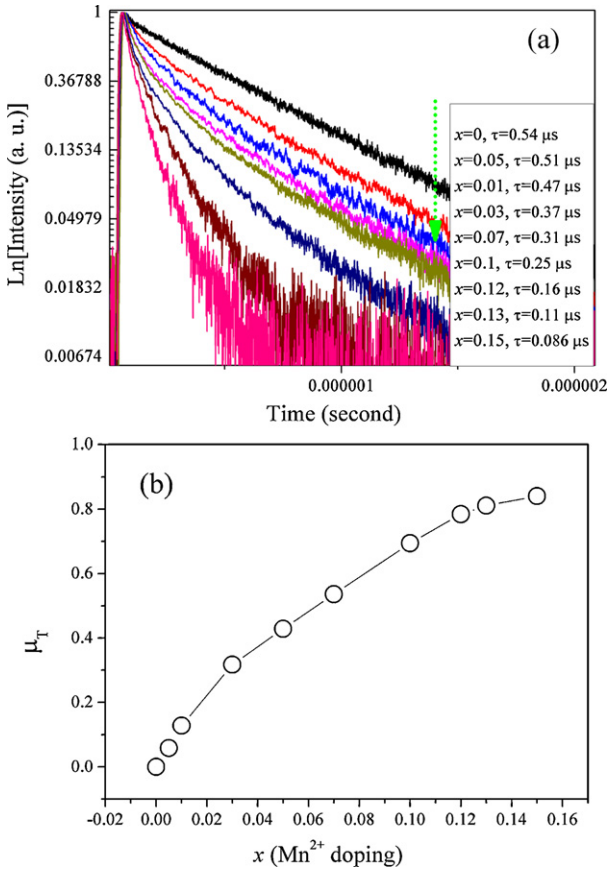

Fig. 7. (a) The luminescence decay curves of $Ba_{1.94}Eu_{0.06}Mg_{1-x}Mn_xP_4O_{13}$ ($x = 0$–0.15) excited at 355 nm and monitored at 430 nm from Eu^{2+} emission; (b) the dependence of energy transfer efficiency on the Mn^{2+} doping level.

where η_{S0} and η_S are the luminescence quantum efficiencies of Eu^{2+} in the absence and presence of Mn^{2+}, respectively; the value of η_{S0}/η_S can be approximately estimated from the luminescence intensity ratio (I_{S0}/I_S); C is the concentration of Mn^{2+}; and $\alpha = 6$, 8, and 10 for dipole–dipole, dipole–quadrupole, and quadrupole–quadrupole interactions, respectively. Thus Eqs. (3) and (4) can be represented by the following equation [24]:

$$\frac{\tau_{S0}}{\tau_S} \propto C^{\alpha/3} \tag{5}$$

Plots of τ_{S0}/τ_S and $\alpha/3$ based on the above equation are also shown in Fig. 8. Linear behavior is observed only when $\alpha = 8$, implying that energy transfer from Eu^{2+} to Mn^{2+} occurrs via the dipole–quadrupole mechanism.

The critical distance R_c for the energy transfer from Eu^{2+} to Mn^{2+} was calculated using the concentration quenching method. The average distance R_{Eu-Mn} between Eu^{2+} and Mn^{2+} can be represented by the equation suggested by Blasse [39]:

$$R_{Eu-Mn} = 2\left(\frac{3V}{4\pi XN}\right)^{1/3} \tag{6}$$

where N is the number of molecules in the unit cell, V is the unit cell volume and χ is the total concentration of Eu^{2+} and Mn^{2+}. If the critical concentration χ_c is used in the above equation, R_c can be obtained. The critical concentration χ_c is defined as, at which the luminescence intensity of Eu^{2+} reduces to half of that for the sample in the absence of Mn^{2+}. It can be derived from Fig. 4 that when the Mn^{2+} content is about 0.03, the luminescence intensity of Eu^{2+} decreases to half. Accordingly χ_c is about 0.04 + 0.03 = 0.07. By taking the experimental and analytic values of V, N and χ_c (497.97 Å^3, 2, 0.07, respectively), the critical distance R_c is estimated by Eq. (6) to be about 18.9 Å.

3.5. The luminescence color and thermal stability

The CIE coordinates for $Ba_{1.94}Eu_{0.06}Mg_{1-x}Mn_xP_4O_{13}$ (x = 0–0.15) phosphors were calculated and are shown in Fig. 9. The luminescence colors for samples with different x-value vary from UV to deep red: (x = 0: 0.148, 0.123), (x = 0.005: 0.108, 0.148),

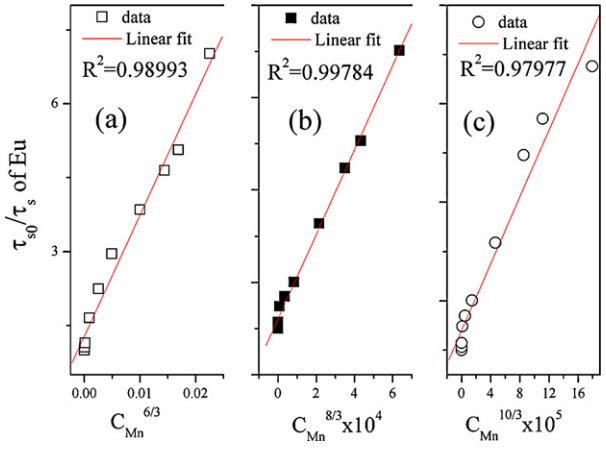

Fig. 8. The dependence of τ_0/τ of Eu^{2+} on (a) $C_{Mn}^{6/3}$, (b) $C_{Mn}^{8/3}$, and (c) $C_{Mn}^{10/3}$.

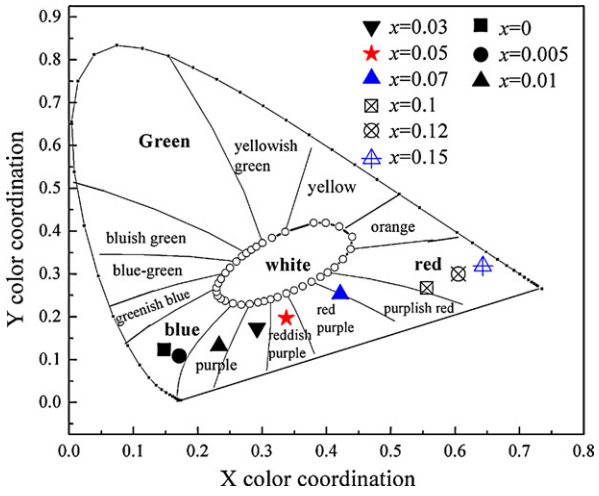

Fig. 9. CIE chromaticity coordinates of $Ba_{1.94}Eu_{0.06}Mg_{1-x}Mn_xP_4O_{13}$ (x = 0–0.15).

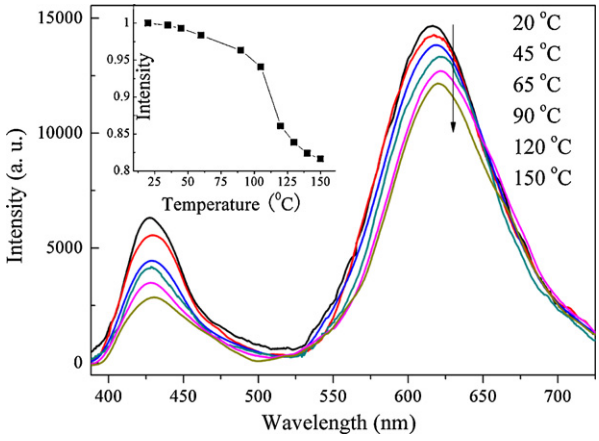

Fig. 10. The emission spectra of $Ba_{1.94}Eu_{0.06}Mg_{1-x}Mn_xP_4O_{13}$ (x = 0.1) from 20 to 150 °C under excitation of 355 nm; the insert is the integrated emission intensity normalized with respect to the value at 20 °C.

(x = 0.01: 0.233, 0.132), (x = 003: 0.292, 0.173), (x = 0.05: 0.337, 0.197), (x = 0.07: 0.421, 0.253), (x = 0.1: 0.556, 0.267), (x = 0.12: 0.605, 0.3), (x = 0.15: 0.643, 0.318).

The temperature-dependent luminescence spectra of $Ba_{1.94}Eu_{0.06}Mg_{1-x}Mn_xP_4O_{13}$ (x = 0.1) are shown in Fig. 10. The weaker peak is originated from the 5d–4f transition of Eu^{2+} ions, and the intense broad emission is from the Mn^{2+} ions. With increasing temperature, the thermal quenching is observed. Inset in Fig. 10 represents the temperature dependence of the integrated emission intensities normalized to the value at 20 °C. The emission intensity at 150 °C is decreased to 82% of the initial value at 20 °C. The results show that the $Ba_{1.94}Eu_{0.06}Mg_{1-x}Mn_xP_4O_{13}$ (x = 0.1) phosphor has a good thermal stability on temperature quenching effect.

4. Conclusions

$Ba_2Mg_{1-x}Mn_xP_4O_{13}$ (x = 0–1.0) and $Ba_{1.94}Eu_{0.06}Mg_{1-x}Mn_x$ ‘P_4O_{13} (x = 0–0.15) phosphors were prepared by conventional

solid-state reaction. The overlap of the emission spectrum of $Ba_2MgP_4O_{13}:Eu^{2+}$ with excitation spectrum of $Ba_2MgP_4O_{13}:Mn^{2+}$ indicates effective energy transfer from Eu^{2+} to Mn^{2+} in $Ba_2MgP_4O_{13}:Eu^{2+},Mn^{2+}$. The emission intensity of $Ba_2MgP_4O_{13}:Mn^{2+}$ peaked at 615 nm is weak. The co-doping of Eu^{2+} as a sensitizer results in a great enhancement of the emission intensity of Mn^{2+}. The optimum concentration of Mn^{2+} with a fixed Eu^{2+} concentration of 3 mol% in $Ba_2MgP_4O_{13}:Eu^{2+},Mn^{2+}$ is about 10 mol%. The CIE chromaticity coordination for $Ba_{1.94}Eu_{0.06}Mg_{1-x}Mn_xP_4O_{13}$ ($x = 0$–0.15) vary from blue to red-purple and eventually to deep red through the energy transfer from Eu^{2+} to Mn^{2+}. The energy transfer from Eu^{2+} to Mn^{2+} is demonstrated to be attributed to an electric dipole quadrupole interaction, and the critical distance is calculated to be about 18.9 Å. The temperature dependence of luminescence shows this phosphor has an excellent thermal stability on the temperature quenching. It is believed that $Ba_{1.94}Eu_{0.06}Mg_{1-x}Mn_xP_4O_{13}$ ($x = 0$–0.15) could be potential for the use in red lamps or W-LEDs.

Acknowledgement

This work was financially supported by the Pukyong National University Research Fund (No. 0012000199602700).

References

[1] C.C. Diao, C.F. Yang, Synthesis of high efficiency $Zn_2SiO_4:Mn^{2+}$ green phosphors using nano-particles, Ceram. Int. 36 (2010) 1653–1657.

[2] X. Qu, L. Cao, W. Liu, G. Su, Preparation and properties of $CdSiO_3:Mn^{2+},Tb^{3+}$ phosphor, Ceram. Int. (2011), doi:10.1016/j.ceramint.2011.05.143, in press, accepted manuscript, Available online 12th June.

[3] I.M. Nagpure, K.N. Shinde, V. Kumar, O.M. Ntwaeaborwa, S.J. Dhoble, H.C. Swart, Combustion synthesis and luminescence investigation of $Na_3Al_2(PO_4)_3$:RE (RE = Ce^{3+}, Eu^{3+} and Mn^{2+}) phosphor, J. Alloys Compd. 492 (2010) 384–388.

[4] U. Happek, A.A. Setlur, J.J. Shiang, Inverse bottleneck in Eu^{2+}–Mn^{2+} energy transfer, J. Lumin. 129 (2009) 1459–1463.

[5] W. Pon-On, S. Meejoo, A. Mehtar, I. Tang, Influence of manganese substitution into the A-site of perovskite type $Ca_{1-x}Mn_xTiO_3$ ceramic, Ceram. Int. 37 (2011) 2075–2079.

[6] E.A. Axtell, J. Hanko, J.A. Cowen, M.G. Kanatzidis, Photoluminescence and magnetism in the new magnetic semiconductors: $K_2Cd_{3(1-x)}Mn_{3x}S_4$, Chem. Mater. 13 (2001) 2850–2863.

[7] F. Tavangarian, R. Emadi, Synthesis and characterization of spinel–forsterite nanocomposites, Ceram. Int. 37 (2011) 2543–2548.

[8] S. Sugano, Y. Tanabe, H. Kamimura, Multiplets of Transition–Metal ions in Crystals, Academic Press, New York, 1970.

[9] T. Moon, G.Y. Hong, H.C. Lee, E.A. Moon, B.W. Jeoung, S.T. Hwang, J.S. Kim, B.G. Ryu, Effects of Eu^{2+} co-doping on VUV photoluminescence properties of $BaMgAl_{10}O_{17}:Mn^{2+}$ phosphors for plasma display panels, Electrochem. Solid-State Lett. 12 (2009) J61–J63.

[10] T.S. Chan, R.S. Liu, I. Baginskiy, Synthesis, crystal structure, and luminescence properties of a novel green–yellow emitting phosphor $LiZn_{1-x}PO_4:Mn_x$ for light emitting diodes, Chem. Mater. 20 (2008) 1215–1217.

[11] W.J. Park, Y.H. Song, J.W. Moon, D.S. Jang, D.H. Yoon, From blue–purple to red-emitting phosphors, $A_{2-x}B_xP_2O_7:Eu^{2+},Mn^{2+}$ (A and B = alkaline–earth metal) under near-UV pumped white LED applications, J. Electrochem. Soc. 156 (2009) J148–J151.

[12] Y. Umetsu, S. Okamoto, H. Yamamoto, Photoluminescence properties of $Ba_3MgSi_2O_8:Eu^{2+}$ blue phosphor and $Ba_3MgSi_2O_8:Eu^{2+},Mn^{2+}$ blue–red phosphor under near-ultraviolet-light excitation, J. Electrochem. Soc. 155 (2008) J193–J197.

[13] S. Ye, X.M. Wang, X.P. Jing, Energy transfer among Ce^{3+}, Eu^{2+}, and Mn^{2+} in $CaSiO_3$, J. Electrochem. Soc. 155 (2008) J143–J147.

[14] J.S. Kim, A.K. Kwon, Y.H. Park, J.C. Choi, H.L. Park, G.C. Kim, Luminescent and thermal properties of full-color emitting $X_3MgSi_2O_8:Eu^{2+},Mn^{2+}$ (X = Ba, Sr, Ca) phosphors for white LED, J. Lumin. 122–123 (2007) 583–586.

[15] T. Aitasalo, A. Hietikko, D. Hreniak, J. Hölsä, M. Lastusaari, J. Niittykoski, W. Stręk, Luminescence properties of $BaMg_2Si_2O_7:Eu^{2+},Mn^{2+}$, J. Alloys Compd. 451 (2008) 229–231.

[16] S. Abe, K. Uematsu, K. Toda, M. Sato, Luminescent properties of red long persistence phosphors, $BaMg_2Si_2O_7:Eu^{2+},Mn^{2+}$, J. Alloys Compd. 408-412 (2006) 911–914.

[17] C.H. Huang, T.M. Chen, A novel single-composition trichromatic white-light $Ca_3Y(GaO)_3(BO_3)_4:Ce^{3+},Mn^{2+},Tb^{3+}$ phosphor for UV-light emitting diodes, J. Phys. Chem. C 115 (2011) 2349–2355.

[18] X. Wang, M. Zhang, H. Ding, H. Li, Z. Sun, Low-voltage cathodoluminescence properties of green-emitting $ZnAl_2O_4:Mn^{2+}$ nanophosphors for field emission display, J. Alloys Compd. 509 (2011) 6317–6320.

[19] C. Zhang, S. Huang, D. Yang, X. Kang, M. Shang, C. Peng, J. Lin, Tunable luminescence in Ce^{3+},Mn^{2+}-codoped calcium fluorapatite through combining emissions and modulation of excitation: a novel strategy to white light emission, J. Mater. Chem. 20 (2010) 6674–6680.

[20] C.H. Huang, W.R. Liu, T.M. Chen, Near UV-pumped yellow-emitting $Sr_8MgSc(PO_4)_7:Eu^{2+}$ phosphor for white-light LEDs with excellent color rendering index, J. Phys. Chem. C 114 (2010) 18698–25649.

[21] N. Guo, H. You, Y. Song, M. Yang, K. Liu, Y. Zheng, Y. Huang, H. Zhang, White-light emission from a single-emitting-component $Ca_9Gd(PO_4)_7:Eu^{2+},Mn^{2+}$ phosphor with tunable luminescent properties for near-UV light-emitting diodes, J. Mater. Chem. 20 (2010) 9061–9067.

[22] C.H. Huang, T.M. Chen, W.R. Liu, Y.C. Chiu, Y.T. Yeh, S.M. Jang, A single-phased emission-tunable phosphor $Ca_9Y(PO_4)_7:Eu^{2+},Mn^{2+}$ with efficient energy transfer for white-light-emitting diodes, ACS Appl. Mater. Interfaces 2 (2010) 259–264.

[23] N. Guo, Y. Huang, H. You, M. Yang, Y. Song, K. Liu, Y. Zheng, $Ca_9Lu(PO_4)_7:Eu^{2+},Mn^{2+}$: a potential single-phased white-light-emitting phosphor suitable for white-light-emitting diodes, Inorg. Chem. 49 (2010) 10907–10913.

[24] C.H. Huang, T.W. Kuo, T.M. Chen, Novel red-emitting phosphor $Ca_9Y(PO_4)_7:Ce^{3+},Mn^{2+}$ with energy transfer for fluorescent lamp application, ACS Appl. Mater. Interfaces 2 (2010) 1396–1399.

[25] Y.N. Xue, F. Xiao, Q.Y. Zhang, A red-emitting $Ca_8MgLa(PO_4)_7:Ce^{3+},Mn^{2+}$ phosphor for UV-based white LEDs application, Spectrochim. Acta A 78 (2011) 1445–1448.

[26] C.H. Huang, P.J. Wu, J.F. Lee, T.M. Chen, $(Ca,Mg,Sr)_9Y(PO_4)_7:Eu^{2+},Mn^{2+}$: phosphors for white-light near-UV LEDs through crystal field tuning and energy transfer, J. Mater. Chem. 21 (2011) 10489–10495.

[27] K.H. Kwon, W.B. Im, H.S. Jang, H.S. Yoo, D.Y. Jeon, Luminescence properties and energy transfer of site-sensitive $Ca_{6-x-y}Mg_{x-z}(PO_4)_4:Eu_y^{2+},Mn_z^{2+}$ phosphors and their application to near-UV LED-based white LEDs, Inorg. Chem. 48 (2009) 11525–11532.

[28] W.R. Liu, Y.C. Chiu, Y.T. Yeh, S.M. Jang, T.M. Chen, Luminescence and energy transfer mechanism in $Ca_{10}K(PO_4)_7:Eu^{2+},Mn^{2+}$ phosphor, J. Electrochem. Soc. 156 (2009) J165–J169.

[29] Z. Hao, J. Zhang, X. Zhang, S. Lu, Y. Luo, X. Ren, X. Wang, Phase dependent photoluminescence and energy transfer in $Ca_2P_2O_7:Eu^{2+},Mn^{2+}$ phosphors for white LEDs, J. Lumin. 128 (2008) 941–944.

[30] Z. Hao, Z. Nie, S. Ye, R. Zhong, X. Zhang, L. Chen, X. Ren, S. Lu, X. Wang, J. Zhang, Luminescence and energy transfer in Eu^{2+} and Mn^{2+} co-doped $Ca_2P_2O_7$ for white light-emitting diodes, J. Electrochem. Soc. 155 (2008) H606–H610.

[31] T.G. Kim, Y.S. Kim, S.J. Im, Energy transfer and brightness saturation in $(Sr,Ca)_2P_2O_7:Eu^{2+},Mn^{2+}$ phosphor for UV-LED lighting, J. Electrochem. Soc. 156 (2009) J203–J207.

[32] N. Xie, Y. Huang, H.J. Seo, A blue-emitting phosphor of $Ba_2MgP_4O_{13}:Eu^{2+}$ for white light UV light emitting diodes, J. Ceram. Proc. Res. 11 (2010) 358–361.
[33] M.V. Hoffman, The systems BaO–MgO–P_2O_5 and BaO–ZnO–P_2O_5, J. Electrochem. Soc. 110 (1963) 1223–1228.
[34] M. Daldosso, D. Falcomer, A. Speghini, P. Ghigna, M. Bettinelli, Synthesis, EXAFS investigation and optical spectroscopy of nanocrystalline $Gd_3Ga_5O_{12}$ doped with Ln^{3+} ions (Ln = Eu, Pr), Opt. Mater. 30 (2008) 1162–1167.
[35] S. Shigeo, M. Yen William, Phosphor Handbook, CRC Press, 1999, p. 171.
[36] I.E.C. Machado, L. Prado, L. Gomes, J.M. Prison, J.R. Martinelli, Optical properties of manganese in barium phosphate glasses, J. Non-Cryst. Solids 348 (2004) 113–117.
[37] P.I. Paulose, G. Jose, V. Thomas, N.V. Unnikrishnan, M.K.R. Warrier, Sensitized fluorescence of Ce^{3+}/Mn^{2+} system in phosphate glass, J. Phys. Chem. Solids 64 (2003) 841–846.
[38] D.L. Dexter, A theory of sensitized luminescence in solids, J. Chem. Phys. 21 (1953) 836–850.
[39] G. Blasse, Energy transfer in oxidic phosphors, Philips Res. Rep. 24 (1969) 131–136.